Statistical Characterization of Urban Spatial Radio Channels

Martin Toeltsch (*Student Member*), Juha Laurila (*Member*)

Kimmo Kalliola, Andreas F. Molisch (*Senior Member*)

Pertti Vainikainen (*Member*), and Ernst Bonek (*Senior Member*)

Abstract

We present a statistical analysis of wideband 3-D channel measurements at base station locations in an urban environment. Plots of the received energy over azimuth, elevation, and delay planes suggest that the incident waves group to clusters in most measured transmitter positions. A super-resolution algorithm (Unitary ESPRIT) allows to resolve individual multipath components in such clusters and hence enables a detailed statistical analysis of the propagation properties. The origins of clusters – sometimes even individual multipath components – such as street apertures, large buildings, roof edges, or building corners can be localized on the city map. Street guided propagation dominates most of the scenarios ($78-97\%$ of the total received power), while quasi line-of-sight over-the-rooftop components are weak ($3-13\%$ of the total received power). For this measurement campaign, in 90% of the cases, 75% of the total received power is concentrated in the two strongest clusters, but only 55% in the strongest one. Our analysis yields an exponential decay of power with $8.9dB/\mu s$, and a standard deviation of the log-normally distributed deviations from the exponential of $9.0dB$. The power of cross-polarized components is $8dB$ below co-polarized ones on average (vertical transmission).

Keywords

Multipath Channels, Radio Propagation, Mobile Radio Channel, Spatial Channel Modeling, Smart Antennas, Clusters.

I. Introduction

Adaptive antennas (AA) will be a major factor for the successful introduction of 3^{rd}-generation wireless systems like UMTS [1], [2], [3], [4]. For the design, performance evaluation, and cell planning with AAs, we need realistic spatial channel models [5], [6]. 3-D measurements are required for parameterization and validation of such channel models.

M. Toeltsch, A. F. Molisch, and E. Bonek are, and J. Laurila was with the Institut für Nachrichtentechnik und Hochfrequenztechnik (INTHF), Technische Universität Wien, Vienna, Austria. E. Bonek is, and A. F. Molisch was also with the Forschungszentrum Telekommunikation Wien (FTW), Vienna, Austria. J. Laurila and K. Kalliola are with the Nokia Research Center, Radio Communications Laboratory, Helsinki, Finland. P. Vainikainen is and K. Kalliola is also with the Institute of Digital Communications (IDC)/Radio Laboratory, Helsinki University of Technology, Espoo, Finland. E-mail: Martin.Toeltsch@ieee.org .

Despite this importance, only few spatial measurements are available, see [7] and references therein. Furthermore, all existing *high-resolution* measurements at the base station (BS) use at most two dimensions, e.g. delay and azimuth [8]. In [9], [10], and [11] wideband 3-D measurements at the mobile station (MS) at street level are reported (downlink measurements). We present here results and analyses of a 3-D measurement campaign *at the BS*, i.e. delay, azimuth, and elevation, and – additionally – polarization. The paper focuses on the statistical evaluation of the data. Details about the measurement setup, the urban environment, as well as sample results and their physical interpretation, are given in [12] and [13]. The evaluation is based on uplink wideband directionally resolved channel measurements in urban macro- and micro-cells in downtown Helsinki, Finland.

Section II introduces the basic concept of array processing, our measurement equipment, and the prerequisites of the synthetic aperture technique. Sec. III describes the environment of the locations, identifies the propagation phenomena, and gives some sample results of the evaluation. In Sec. IV we describe and discuss the statistical analysis, finally Sec. V summarizes this paper.

II. Measurement Setup

To determine the parameters of the incident waves, we used a wideband channel sounder together with a planar antenna array. The measurements were performed by the Institute of Digital Communications (IDC) of the Helsinki University of Technology (HUT) in cooperation with the Institut für Nachrichtentechnik und Hochfrequenztechnik (INTHF) of Technische Universität Wien with the IDC wideband channel sounder [14] utilizing a switched multiplexing principle introduced in [15]. The center frequency was $2154MHz$, the measurement bandwidth was $100MHz$. The transmitter sent a PN-sequence with 255 chips continually, i.e. starting the same sequence again immediately after the end of the last one. The chip frequency of the transmitter was $30MHz$, the sampling frequency of the analog-to-digital converter was $120MHz$, from which follows that each chip was four times oversampled at the receiver. It used a PN-sequence correlation technique for the determination of the impulse response. Hence, the delay range is $255/30MHz = 8.5\mu s$ with a resolution of $1/30MHz = 33ns$.

The transmit antenna at the mobile station (MS) was a vertically polarized omnidirectional discone antenna. The vertical 3dB-beamwidth was 87°, the transmit power $40dBm$. Approximately 80 different transmitter positions were investigated.

The receiving base station was located at one of three different sites below, at, and above the rooftop level (RX1 – RX3, cf. Fig. 1). A 16-element physical array with dual polarized $\lambda/2$-spaced patch antennas was combined with

a synthetic aperture technique to build a virtual 2-D antenna structure. The patches were linearly polarized at 0° (horizontal direction) and 90° (vertical direction). With these 16×62 elements we are able to resolve the direction of arrival (DOA) of incoming waves both in azimuth (horizontal angle) and elevation (vertical angle) by using the super-resolution Unitary ESPRIT algorithm [16], [17], [18]. Note that the number of antenna elements limits the number of identifiable waves, but not the angular resolution of the method. Together with a delay resolution of $33ns$ we are able to characterize the radio channel in all 3 dimensions separately for the two polarizations. An excellent overview about array signal processing – including estimation of the DOAs and a comparison of ESPRIT with other algorithms – can be found in [19].

One prerequisite for the applicability of the synthetic aperture technique is that the radio channel is static during the whole data collection period. The time for one complete measurement was $14.5s$. We tested the impact of moving cars by performing several measurements at the same position with and without traffic. The traffic caused variations of up to 20% of the angular power spectrum, whereas 2 consecutive measurements without traffic only showed 5% variation. From that we can conclude that the repeatability is very good in the absence of traffic, and that the impact of moving objects can be shown and also be quantified. To avoid problems, the whole procedure was done at night with minimum traffic conditions.

III. Propagation Environments

A. Description of environment

We performed the measurements in an urban environment in downtown Helsinki, Finland, in June and October 1999. The three receiver locations (RX 1–3) are marked in Fig. 1 by triangles pointing in broadside direction of the array. The photos of the Figures 2, 3, and 4 have the same viewing direction. Figure 1 also informs about all the corresponding TX positions. The location RX 1 (height $h_{RX} = 10m$) was a typical microcell site below the rooftop height of the surrounding buildings, and we performed measurements with 20 different TX positions. RX 2 (height $h_{RX} = 27m$) was at the rooftop level, and we investigated 32 TX positions. RX 3 (height $h_{RX} = 21m$) was a typical macrocell BS position above rooftop heights, and we measured at 27 TX positions. More information on the locations and the environment can be found in [12]. Note that even if we are talking about macrocells (RX 3), the distances between transmitters and the receiver were still below $500m$.

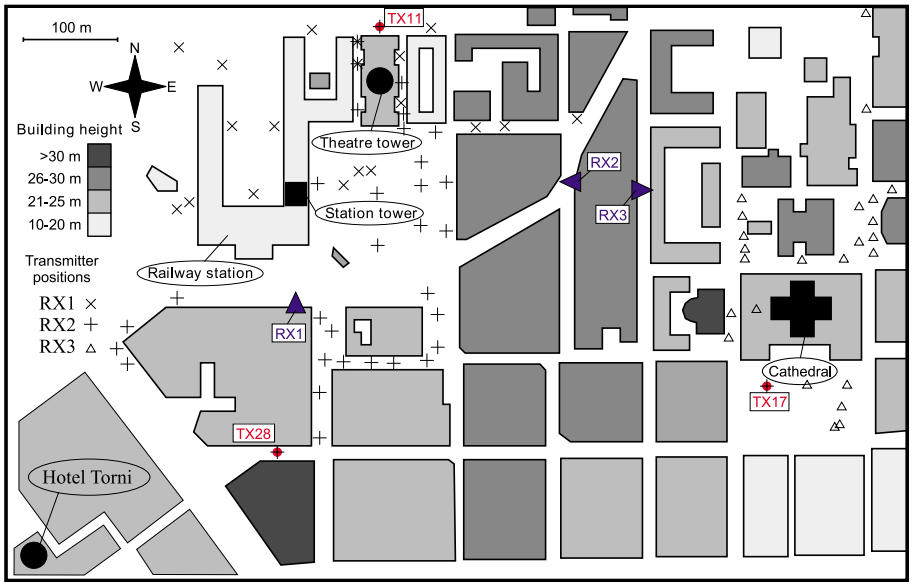

Fig. 1. Overview about the measurement area with all 3 RX sites, the TX-positions of the sample plots are marked by red color

A.1 RX1

Characteristic for this site is the wide and open square in front and slightly to the right of the array (Rautatientori). The square is surrounded by relatively high buildings[1] that are intersected by alleys and narrow streets. To the front left of the antenna is the large railway station, the entrance is at an azimuth $\varphi \approx -40°$. The station tower directly in front of RX1 at 0° is the highest building in the vicinity. Behind the railway station is a large railway yard. Figure 2 shows a view from RX1 to the square.

A.2 RX2

The view from RX2 shows the dominating street canyon of the broad Kaisaniemenkatu approaching the receiver from the left at $-30°$ (see Fig. 3). On the other end of the street is the large Rautatientori square (cf. Sec. III-A.1), where electromagnetic energy is easily coupled into the street canyon. The height of this RX site is at the rooftop level of the surrounding houses. In several directions high rise buildings and towers can be seen (LOS from RX2 to them), e.g. Theatre Tower, White Tower (cf. Figure 2), Hotel Torni, World Trade Center (WTC), Makkaratalo building (M'talo).

A.3 RX3

Although the height of RX3 is lower than that of RX2, it is an above-rooftop-site, as the buildings in front are significantly lower. The dominating Lutheran Cathedral with its metallic dome at $\varphi \approx 40°$ to the right acts as a strong

[1] Most of them have 4 floors

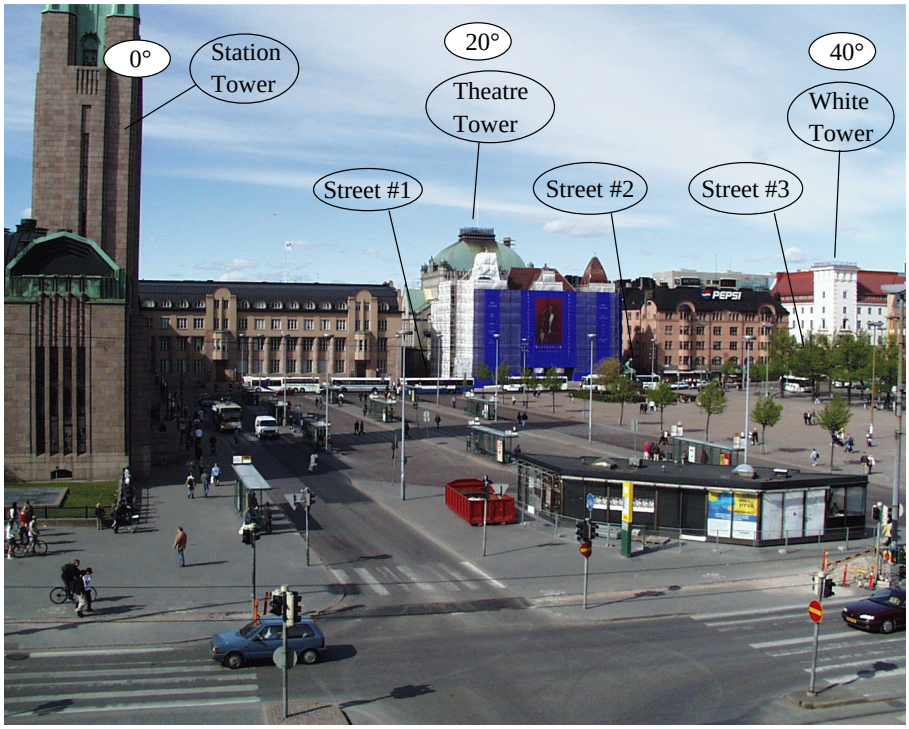

Fig. 2. View from RX1 site (microcell)

scatterer, see Fig. 4. South of the cathedral is a large square (Senate Square) without LOS to the receiver.

B. Sample results

In this section we show some graphical results of the DOA estimation with Unitary ESPRIT. The power of the multipath components is calculated by means of a beamforming algorithm. From the approximately 80 transmitter positions, we choose representative ones, where several different propagation mechanisms become obvious. We mark concentration of strong multipath components by black ellipses and denote the objects (e.g. Street Canyon, Theatre, ...) that originate them.

Note that the plots show the sum of the powers in horizontal and vertical polarization. Due to the continuously transmitting mobile station, the delay can only be interpreted as a relative distance between multipath components. The TX-positions used in the sample plots are marked in Fig. 1. TX 11 stands for the positions TX 9–14, which are all near TX 11.

B.1 Transmitter Position TX 9–14 (RX 1)

These TX positions were located in the street canyons behind the large square about $300m$ distant from the receiver array (RX 1), see also the photo in Fig. 2 (*Street #1, Street #2*). Figure 5 shows the received power at the base station

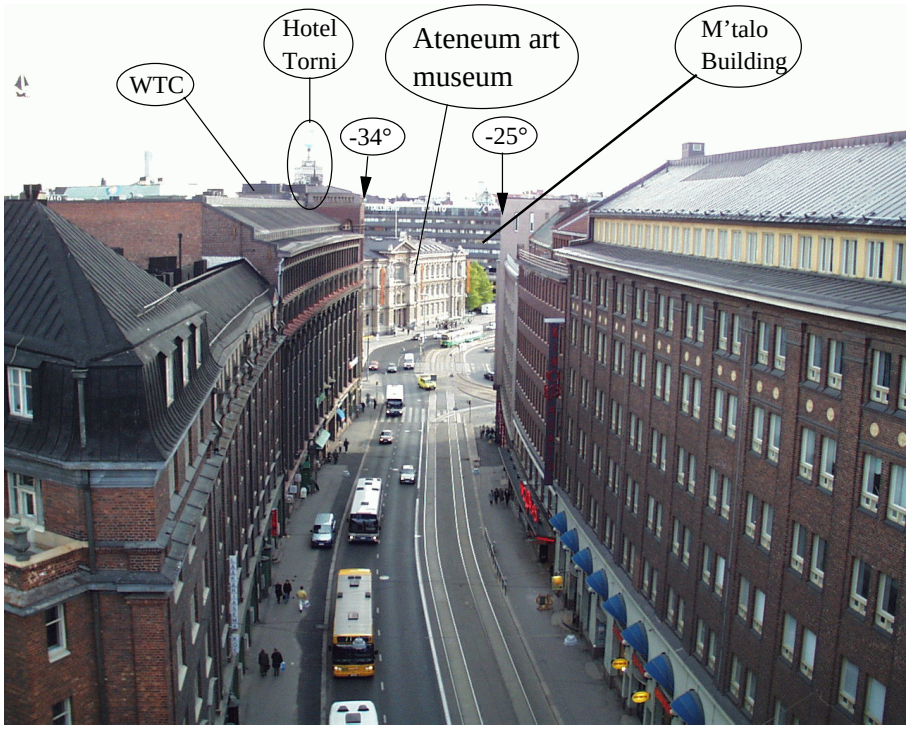

Fig. 3. View from RX2 site (macrocell)

site RX 1 over the azimuth-elevation plane. The plot is color-coded, the brighter the color the stronger the power of incident waves. The minimum size of the "diamonds" corresponding to an individual wave has been chosen for optimum visibility in the plot. It is *not* related to the angular resolution! The power of both the horizontal and the vertical components of the six transmitter positions (TX 9–TX 14) is summed up. This averaging gives a better picture of the propagation from a (small) area than by one TX position alone.

We can observe that the energy is concentrated in *clusters* that correspond to objects in the surrounding. Different propagation mechanisms also became evident, e.g. street-guided propagation (*Street #1, #2, and #3*), reflection on high-rise buildings (*Theatre Tower*), diffraction at the edge of a wall (*Railway Station Corner*), or scattering on surrounding buildings on the right-hand side of the square after street guidance (*Right-hand side*).

B.2 Transmitter Position TX 28 (RX 2)

TX 28 is situated behind a large block at a distance of 420m from the receiver (RX 2), so there is no line-of-sight (LOS) from the transmitter to the receiver, but there is a LOS-connection from the transmitter to the Hotel Torni, which in turn has LOS to the receiver array at the azimuthal angle of $\varphi \approx -36°$.

Figures 6 and 7 show the power over the azimuth-elevation and azimuth-delay planes, respectively. In the delay domain

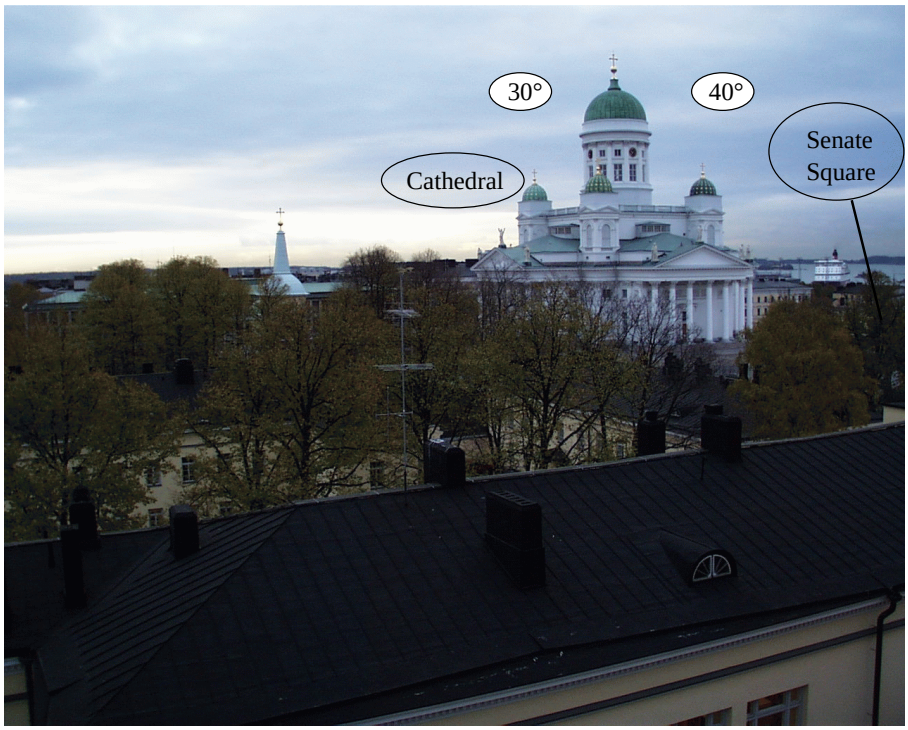

Fig. 4. View from RX3 site (macrocell)

we identify 3 parts. The first components arrive from the direction of the transmitter over the rooftop ($-41°/+1°$, azimuth/elevation) (*Pseudo LOS*) with some weaker components coming also from the street canyon in front of the array (*Street Canyon (1)*). The second component is also coupled into the broad Kaisaniemenkatu street, but with a delay of $0.6\mu s$ and an elevation of 0° (*Street Canyon (2)*). The higher elevation indicates that these waves are apparently diffracted over the roof of the Ateneum art museum at the end of the Kaisaniemenkatu street (cf. Figure 3). The last component is a reflection from the Hotel Torni ($-35°/2\ldots3°$), and it carries about $8dB$ more power than the other components.

We again observe a strong grouping of waves into *clusters*. At the position of these clusters in the azimuth-elevation-delay domain, important objects like street canyons or large buildings can be identified.

B.3 Transmitter Position TX 17 (RX 3)

TX 17 is located on the Senate Square south of the large cathedral, $240m$ from the receiver (RX 3); there is no LOS to the receiver.

We show azimuth-elevation and azimuth-delay plots in Figures 8 and 9, resp. There is no early component from the direction of the transmitter (56°), the first wave is seen in the direction of a street crossing (*Street Guidance*). A

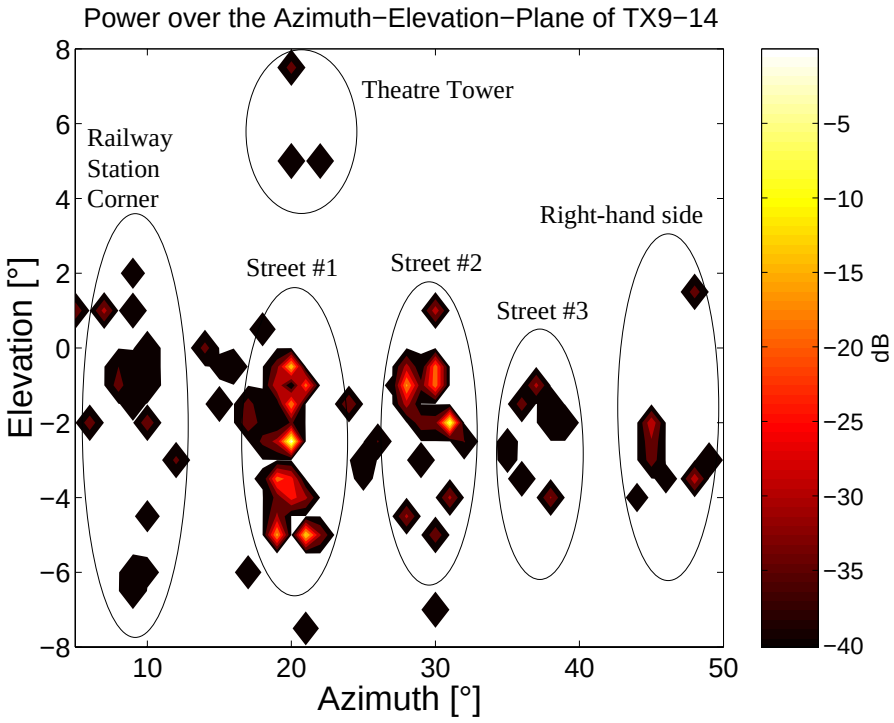

Fig. 5. Azimuth-elevation plane, sum of the powers of the co- and cross-polarized component of TX9–14

reflection from the metallic dome of the cathedral (*Metallic Dome*) arrives with a short delay. $0.6\mu s$ ($180m$) after the first waves, there are several reflections from the houses behind the square, where the cathedral blocks the energy in the azimuthal range $28 \ldots 40°$ (*Around Cathedral, Reflections*).

C. Some comments about propagation

In Section III-B, we show that it is possible to identify many single (particular, different) multipath components, impinging at the receiver from different directions. But these components are not randomly distributed in the spatial and temporal domain, they naturally group to *clusters*. These clusters can be associated with objects in the environment due to the high angular and temporal resolution of our evaluation. (Sometimes even individual waves, within a cluster, can be associated with scattering objects.) The identification of such clusters is facilitated by inspection of the maps of the environment.

We define a cluster as a group of waves whose delay, azimuth, and elevation at the receiver are very similar, while being notably different from other waves in at least one dimension. Additionally all waves inside a cluster must stem from the same propagation mechanism.

We note at this point that the definition of clusters always involves a certain amount of arbitrariness. Even for

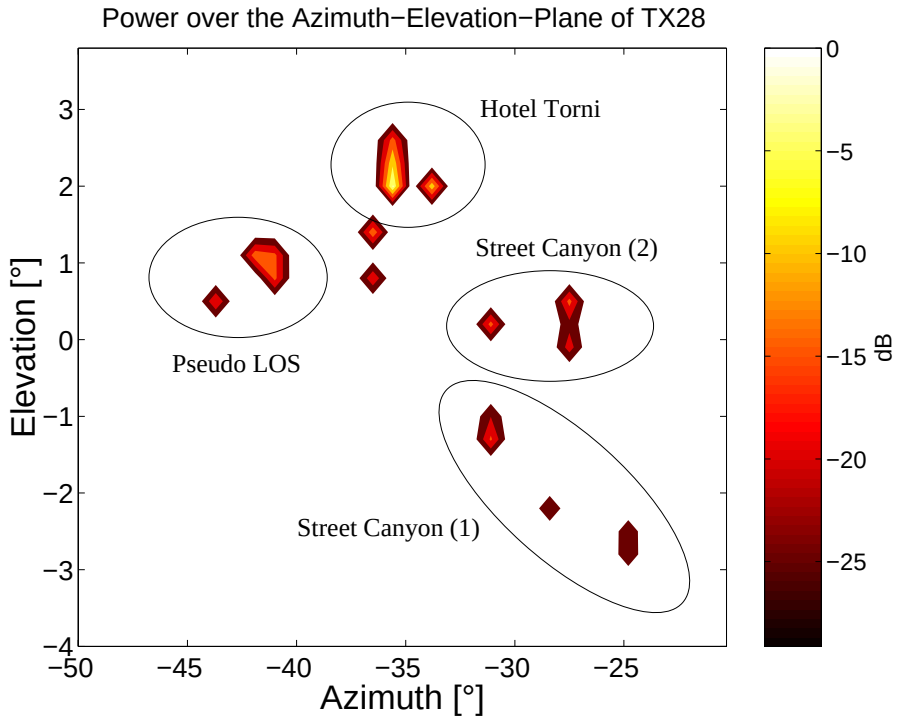

Fig. 6. Azimuth-elevation plane, sum of the powers of the co- and cross-polarized component of TX 28

mathematically "exact" definitions, arbitrary parameters (e.g. thresholds or number of components) must be defined. Clustering by human inspection, supported by maps of the environment, seems to give the best results.

We calculated the received power within each cluster (*cluster power*) by means of Unitary ESPRIT and a following beamforming algorithm. The results were plotted in the azimuth-elevation-, azimuth-delay-, and elevation-delay-planes, samples can be seen in Section III-B. According to the obvious propagation mechanism, we assigned each clusters to one of three different classes.

Class 1: Street-guided propagation

Waves arrive at the receiver from the street level after traveling through street canyons. A typical example is the broad Kaisaniemenkatu street of RX 2.

Class 2: Direct propagation - over the rooftop

The waves arrive at the BS from the rooftop level by diffraction at the edges of roofs, either directly or after reflection from buildings surrounding the MS. The azimuth mostly points to the direction of the transmitter with some spread in azimuth and delay. As an instance of Class 2, TX 10 – TX 20 at RX 3 (west and south of the cathedral, all close to TX 17 in Fig. 1) can be mentioned.

Class 3: Reflection from high-rise objects – over the rooftop

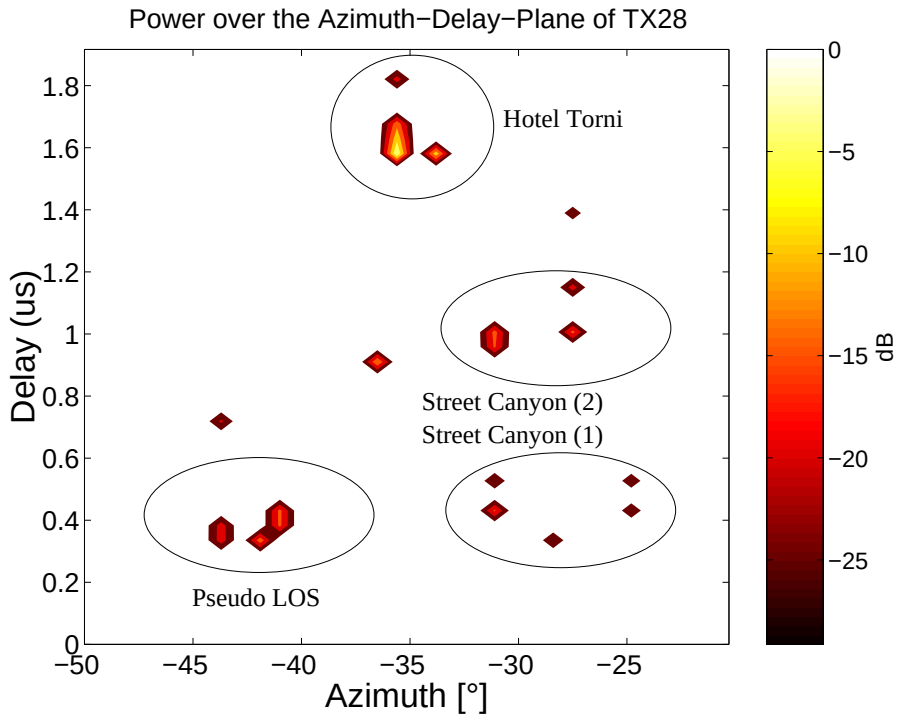

Fig. 7. Azimuth-delay plane, sum of the powers of the co- and cross-polarized component of TX 28

The elevation angles are near the horizon, pointing at or above the rooftop. The waves undergo a reflection at an object rising above the average building height before reaching the BS. The azimuth shows the direction of the reflecting building, the delay is typically larger than for Class 1 or Class 2. One example for such a reflector is the Lutheran Cathedral at RX 3.

The sum of the powers of all clusters belonging to the same class is called *class power*. In some cases the propagation history is a mixture of different classes, e.g. street guidance followed by diffraction at rooftops. We allocated such clusters to the class of the final path to the BS [2].

IV. Statistical Analysis

In Section III we showed by several sample plots that the waves received by the base station emanate from concentrated clusters. These clusters are present in the delay- as well as in the azimuth- and elevation-domains.

In the current section, we present some statistical evaluation to substantiate and quantify the clusterization. We will investigate (i) the number of clusters that is required to get a specific percentage of the total power, (ii) the powers of the clusters vs. the delay, (iii) the cross polarization discrimination (XPD) vs. the delay, (iv) the relative class powers, and (v) the distribution of the number of clusters. Such questions are important for designing algorithms for adaptive

[2]Double-directional channel measurements [20] allow the tracing of up to three reflections or diffractions.

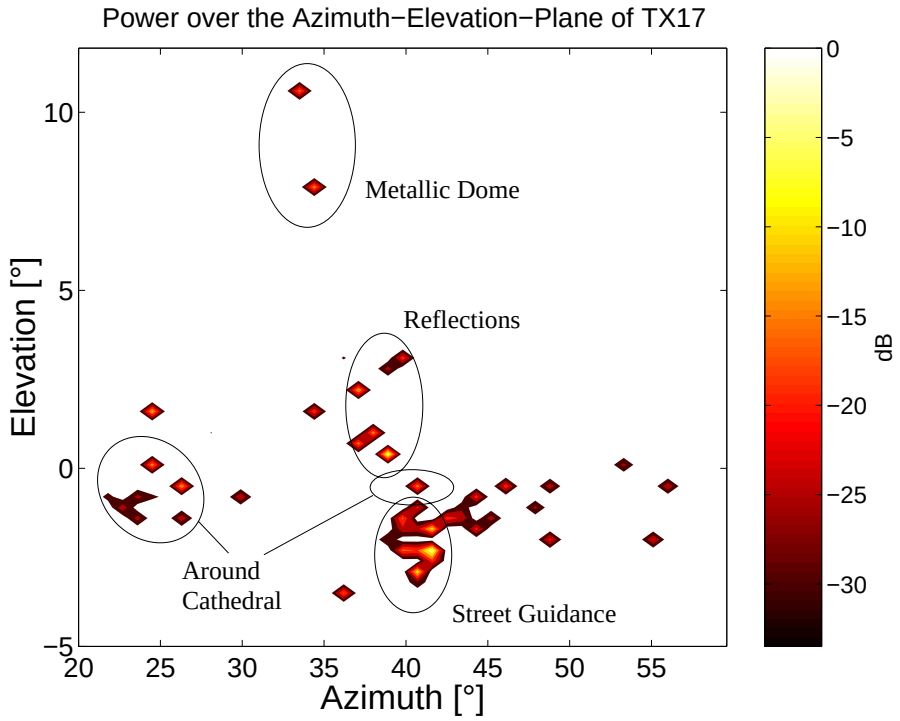

Fig. 8. Azimuth-elevation plane, sum of the powers of the co- and cross-polarized component of TX 17

antennas, e.g. should one capture, in uplink, the power of one or more clusters; or, in downlink, how to distribute the available transmit power to which directions?

A. CDF of Relative Power

We sorted the clusters of each TX position in descending order of their received power. After that we calculated the ratio of the strongest-cluster power to the total received power; then the same for the sum of the first two clusters, the first three clusters, and so on. To generate a cumulative distribution function (cdf) of the relative power, we combined the results of all TX positions. Figure 10 shows the cdf of the relative power for 1 to 4 clusters for the case of vertical polarized transmitted and vertical polarized received signals (VP-VP). In Fig. 11 the same is plotted for the horizontal (cross-) polarized received component (VP-HP)[3]. In the legends, we specify the number of samples the cdf's are based on.

First, we answer the question, how many percent the power of the *strongest* cluster contributes to the total power. If we refer to the 10% level in the cdf, Figure 10 (11) says that in 90% of all cases the power in the strongest cluster is at least 55% (40%) of the total power. The average power of all strongest clusters of the measurements is $0.8dB$ (co-polarized) and $1.1dB$ (cross-polarized) below the total power, that is 83.2% and 77.6% of the total power. The average

[3]Note that the transmitter always sent vertically polarized.

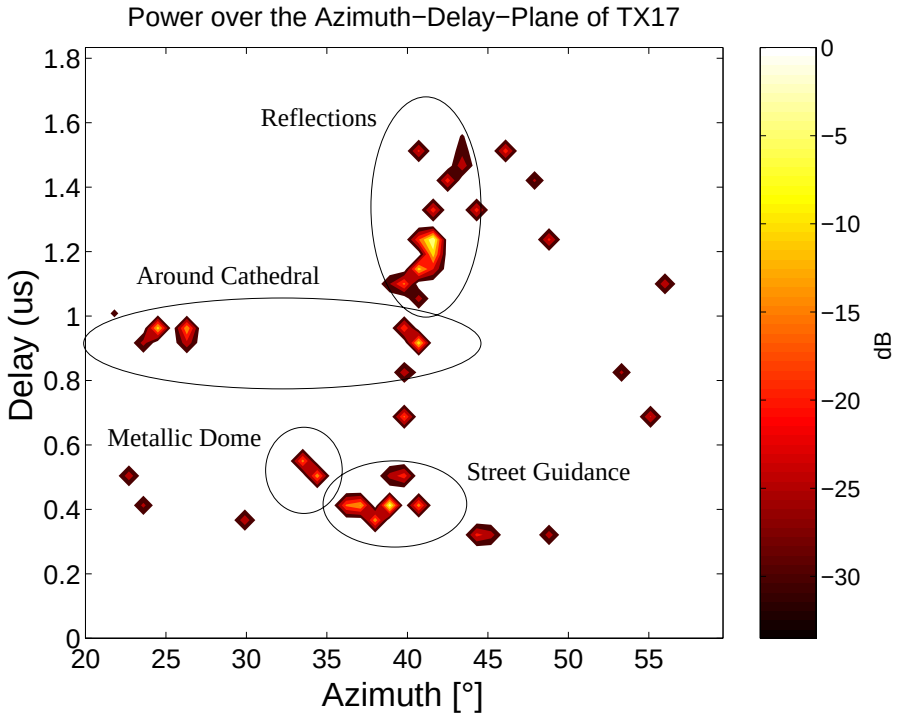

Fig. 9. Azimuth-delay plane, sum of the powers of the co- and cross-polarized component of TX 17

extent of the strongest cluster is 23° (10°) in azimuth (elevation); the corresponding standard deviation is 18° (5.5°). Pointing a single beam – whose beam width has to match this extent – to capture the strongest cluster only, means losing about $2.6dB$ or less of the available power in 90% of the cases. The average loss is only $0.8dB$. Note that the average size of a cluster is in general different from the intracluster spread [21]. Table I shows the average attenuation of the strongest cluster separately for the RX-sites. In particular at RX 2, the energy is exceedingly concentrated inside the

RX	VP-VP dB (% of P_{tot})	VP-HP dB (% of P_{tot})
1	-0.9 (81%)	-1.2 (76%)
2	-0.4 (91%)	-0.6 (87%)
3	-1.3 (74%)	-1.8 (66%)

TABLE I

Average relative power in dB (relation of cluster power to total received power P_{tot}) of the strongest cluster of RX1, RX2, and RX3, and the ratio in %

strongest cluster (91% and 87% of the total received power) due to the guidance of Kaisaniemenkatu street's aperture.

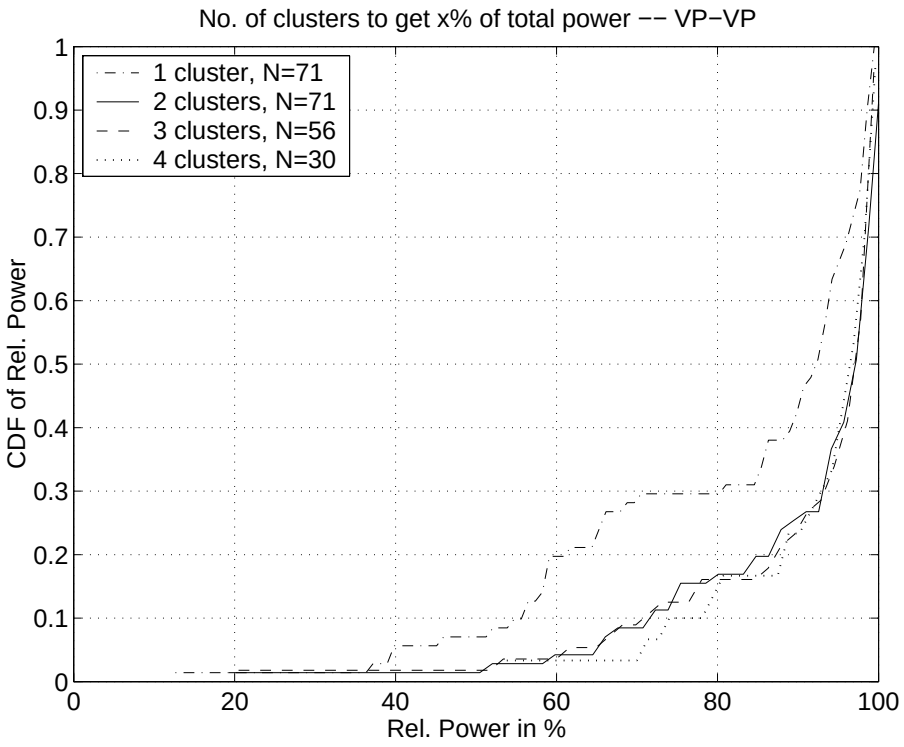

Fig. 10. CDF of the relative power for 1–4 clusters, all TX positions, transmitter and receiver vertically polarized (VP-VP). N is the number of samples.

Secondly, we analyze the contribution of the two strongest clusters. If we refer again to the 10% level in the cdf, Figure 10 says that now 75% of the received, vertical power (VP-VP) is concentrated in the 2 strongest clusters, whereas the residual 25% is not concentrated in clusters anymore. It does make a difference to employ one or two clusters, but not more. For the cross-polarized component (VP-HP) the collected power increases to 60% if we use the 2 or 3 strongest clusters. With 4 clusters, 90% of the total power can be captured. The difference between 2, 3, and 4 clusters vanishes for higher levels of the cdf ($85 - 92\%$ at a cdf-level of 0.2).

Finally, we compare the relative importance of the 3 classes defined in Section III-C. Figures 12, 13, and 14 show the cdf of their relative power. We only show the VP-VP case. Again, we specify the number of samples the cdf's are based on in the legends. We recognize the importance of class-1 clusters (street-guided propagation). In 50% of all class-2 and class-3 clusters the relative power is less than 10%, even for the sum of the 3 strongest clusters of each TX-position. Note that the separation into the 3 classes for the 3 strongest clusters (Fig. 14) yields only few samples for the corresponding cdf and hence it is not very smooth anymore. Nevertheless, what can be observed is that there are far less class-2 clusters (direct over the rooftop) than class-1 or class-3. Moreover, the contribution of class-2 clusters to the total power is in all cases almost negligible compared to the other classes.

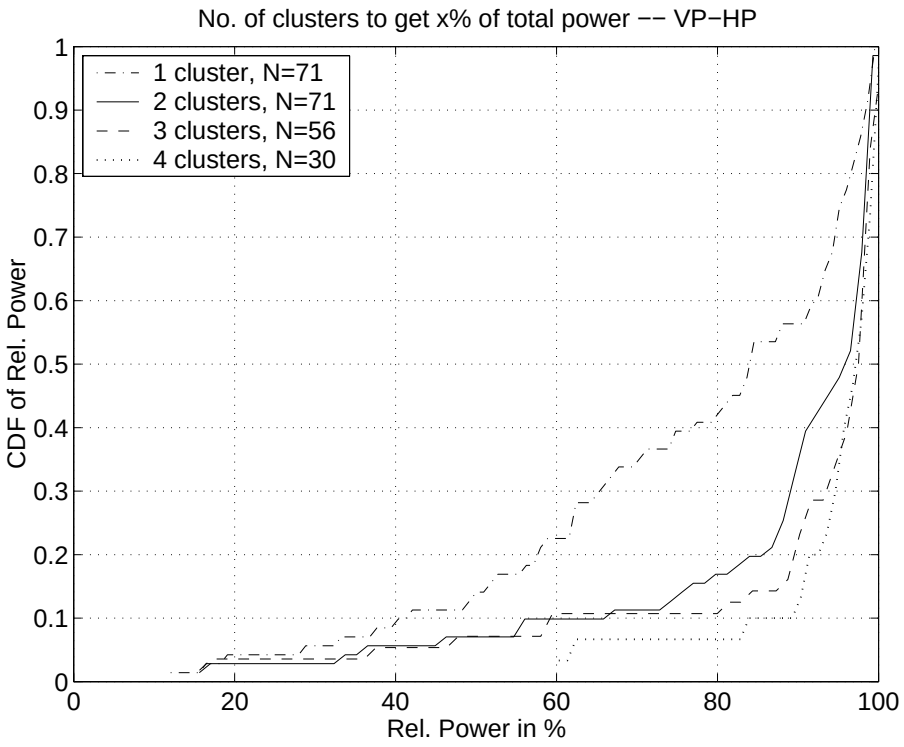

Fig. 11. CDF of the relative power for 1–4 clusters, all TX-positions, transmitter vertically and receiver horizontally polarized (VP-HP). N is the number of samples.

Our investigation reveals that (i) significant power comes from narrow angle ranges (clusters), and (ii) there are several such clusters present. Especially the more important co-polarized waves (VP-VP) are concentrated by at least 75% in the 2 strongest clusters ($-1.2dB$ of the total power).

B. Cluster powers vs. delay

We assigned each cluster its mean delay and related its cluster power to the total received power of the corresponding TX-position to get the *cluster attenuation*. The mean delay is the power-weighted average of the excess-delays of all multipath components in the cluster. The mean delay values of the clusters are always given relative to the mean delay of the first clusters, i.e., we assign a delay of $\tau = 0ns$ to the first cluster. The quantity of interest is the relationship between cluster power and delay. Simple propagation models postulate an exponential law [22]. In analogy, we define $P_i \propto ae^{-\tau_i/b}$, where P_i is the linear power of cluster i (P_i not specified in dB!) and τ_i is the delay of cluster i. a and b are model parameters, where b denotes the mean power decrease per delay unit and a is the average of the powers at zero delay (quasi line-of-sight components). We estimated the parameters a and b by a least-squares (LS) fit of the exponential law to the measured powers. Appendix A describes this estimator. The Figures 15 and 16 show the scatter plot of (attenuation, delay)-tuples. The total number of clusters were 255 and 233, resp. All calculations are done with

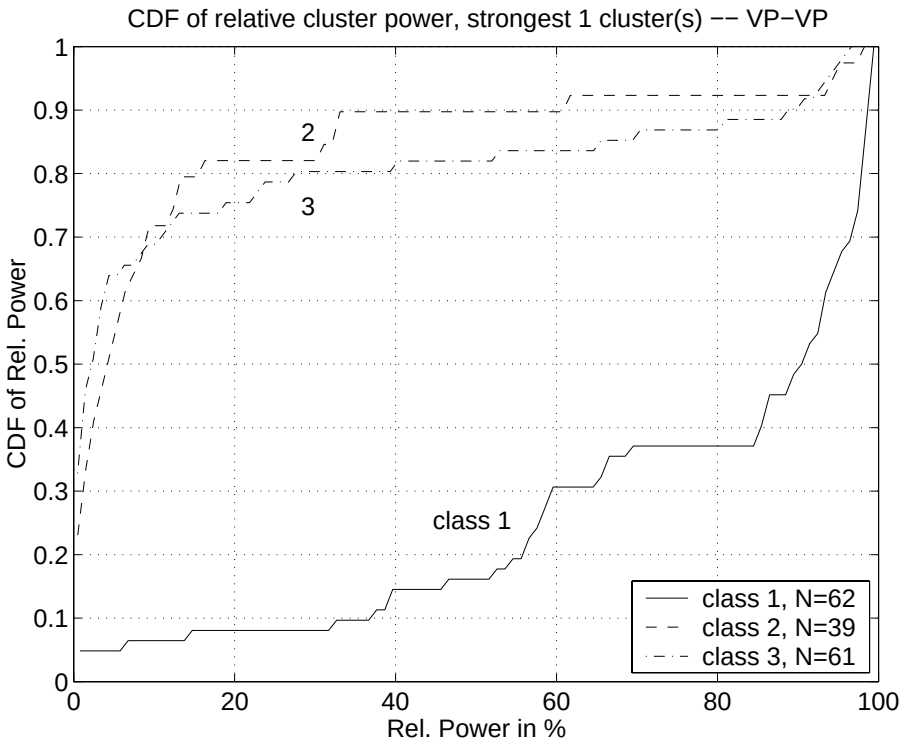

Fig. 12. CDF of the relative power for the strongest cluster separated by classes, all TX-positions. N is the number of samples.

linear powers; on the other hand, for visualization we prefer a logarithmic scale of the figures. By that we demonstrate two different interesting results. (i) These figures also show the LS fit to an exponential, which appears as a linear line in the logarithmic scale. We emphasize that it is different from a linear regression between the powers in dB and the delays. The slope of this line – corresponding to the model parameter b – explains the decreasing power of the clusters with increasing delay. Table II shows the parameter values for a and b. (ii) Furthermore, we show the moving average

	VP-VP	VP-HP
a	$-3.9dB$	$-3.6dB$
b	$8.9dB/\mu s$	$11.8dB/\mu s$

TABLE II

The model parameters a and b for both received polarizations (VP and HP) averaged over all available clusters. The transmitter was vertically polarized (VP).

of the linear cluster powers in a $\pm 67ns$ delay window and the standard deviation σ_v of the estimation error v in the delay window in a distance of $\pm 1\sigma$ from the power average (the mathematical definitions of v and σ_v are also given in Appendix A). We define σ_v as the standard deviation of the logarithmic estimation error in dB. This estimation

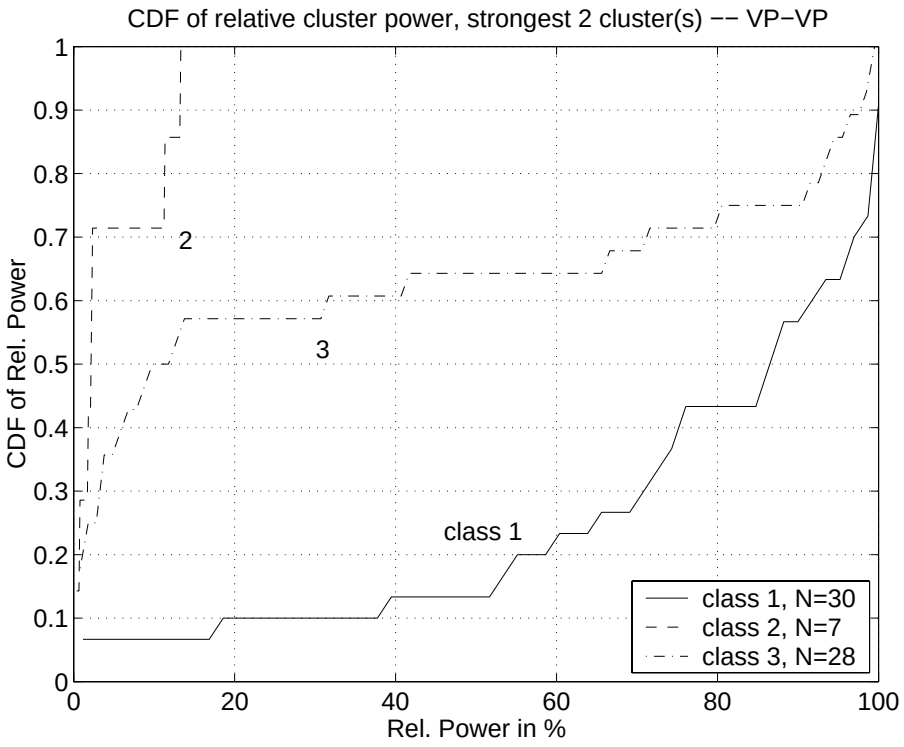

Fig. 13. CDF of the relative power for the 2 strongest clusters separated by classes, all TX-positions. N is the number of samples.

error was found to be log-normally distributed and up to a delay of about $1\mu s$, σ_v is independent of the delay τ. The value of σ_v is $9.0dB$ and $10.0dB$ (co- and cross-polarization), resp., averaged over the first microsecond. After $1\mu s$ there are too few clusters to draw reliable conclusions. Neither the moving average nor the standard deviation are plotted in sections where are too few data samples, e.g. at $\tau \approx 1.5\mu s$ in the horizontal case (VP-HP). The averaged attenuation of all shortest delayed clusters corresponds to the parameter a of Tab. II.

The cumulative distribution function of the delay of all strongest clusters shows that, in 60% of the cases, it is the quasi line-of-sight component that carries the largest power. The remaining 40% of the clusters is equally distributed between 0 and $1\mu s$ excess delay. The first cluster is not necessarily the strongest one. The mean values of the delays of those clusters that carry the strongest co- and cross-polarized energy are $0.21\mu s$ and $0.15\mu s$, resp. In Tab. III we summarize the average delay values separately for each RX-site. Whereas the excess path length of the strongest cluster of RX 1 and RX 3 (compared to the first cluster) is in the order of $15 - 30m$, it is more than $100m$ in the case of RX 2. This corresponds well to the length of the broad Kaisaniemenkatu street ($120m$) in front of the receiver array. The first components are from the quasi line-of-sight direction, but – in contrast to RX 1 and RX 3 – only few of them carry large power. The strongest waves are coming through the street aperture and have an excess delay corresponding exactly to the length of the street!

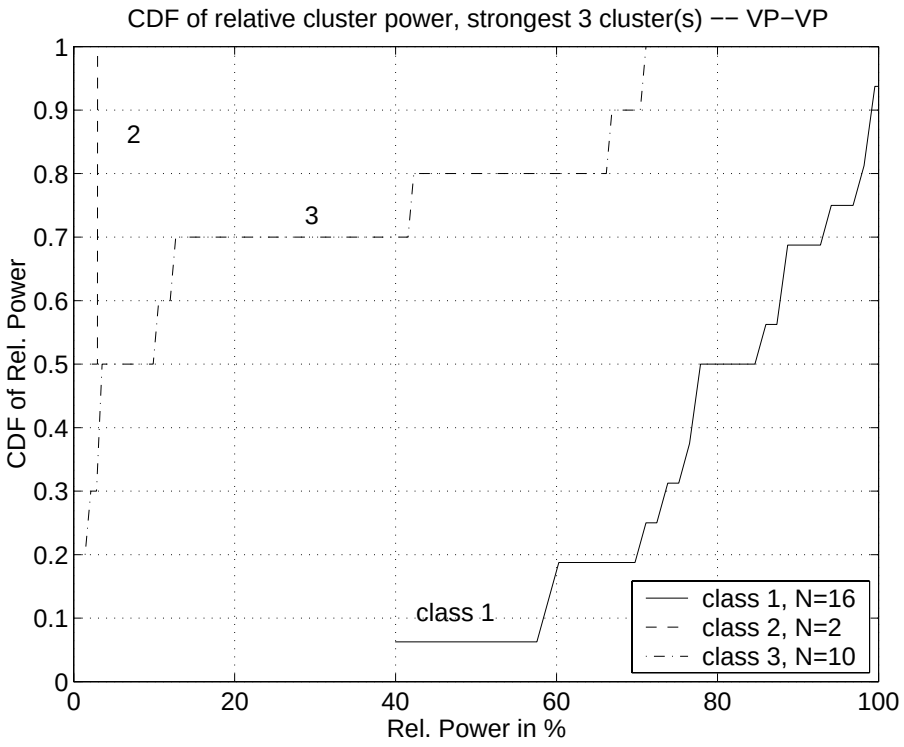

Fig. 14. CDF of the relative power for the 3 strongest clusters separated by classes, all TX-positions. N is the number of samples.

RX	av. delay VP-VP μs	av. delay VP-HP μs
1	0.068	0.071
2	0.38	0.28
3	0.11	0.048

TABLE III

AVERAGE DELAY OF THE STRONGEST CLUSTER OF RX 1, RX 2, AND RX 3.

C. Cross polarization discrimination vs. delay

The cross polarization discrimination (XPD) is defined as the ratio of the received power of the co-polarized component to the power of the cross-polarized component, evaluated for each cluster. Instead of approximating the linear values as done in Sec. IV-B, we applied the linear least-squares estimate of the logarithmic XPD in dB to equally weight positive and negative values. The linear regression of the XPD in dB vs. the delay should again give information about the correlation between the two variables. In Fig. 17 each XPD-value is marked by an asterisk at its corresponding delay. The number of clusters in this figure is N=215. The linear regression has a slope of $1.4 dB/\mu s$, hence with increasing

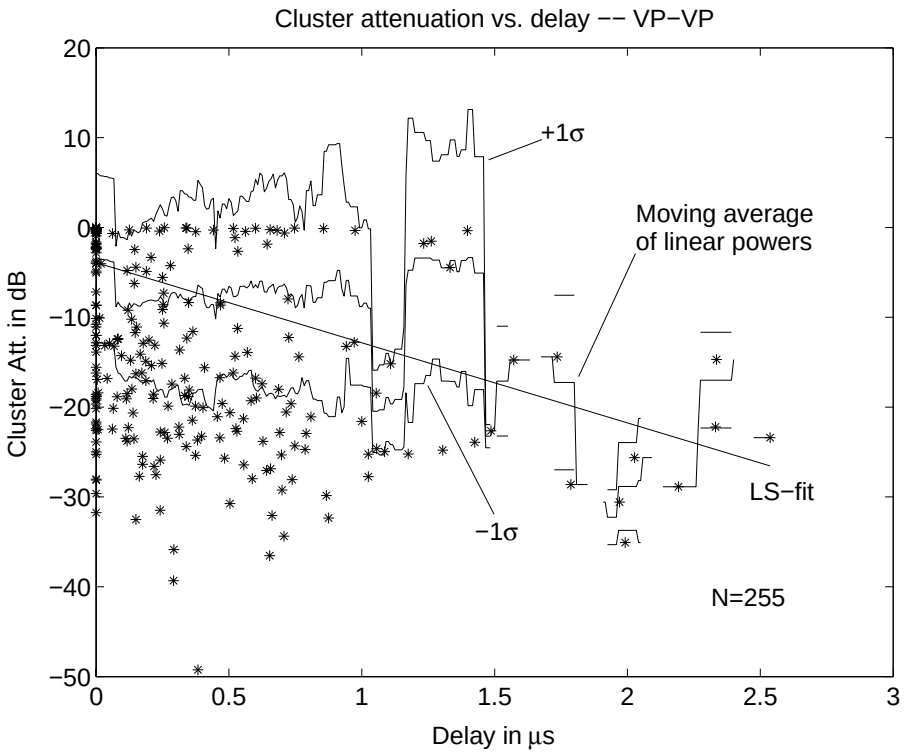

Fig. 15. Relation of the cluster power to the total power vs. delay, all TX-positions, Co-Polarization. N is the number of clusters.

delay the co-polarized component (VP-VP) gets stronger compared to the cross-polarized component (VP-HP). Again we also plot the moving average of the XPD in a $\pm 67ns$ delay window and the upper and lower $\pm 1\sigma$ standard deviation curve. Here, σ is the standard deviation of the measured XPD-data from the linear regression line. It significantly reduces from about $\pm 10dB$ below $\tau = 0.5\mu s$ to $\pm 3dB$ above $\tau = 0.5\mu s$. I.e., with increasing delay the XPD increases, and the samples are strongly concentrated around their average. In most of the cases (89%) the vertical component is much stronger than the horizontal, the average of all XPD-values is $8.0dB$.

In Figure 18, we show the cumulative distribution function (cdf) of the XPD separately for the three different classes 1–3 (cf. Section III-C). The legend also denotes the number of clusters in the corresponding classes. The XPD of all class-1 clusters (street-guidance) is on average 5 dB greater than the class-2 (over the rooftop) and class-3 clusters (far reflections). Referring again to the 10%- level of the *cdf*, we observe a 5 dB difference between class-3 and class-2 clusters, as well as between class-2 and class-1 clusters. The conclusion is that street guidance seems to preserve the polarization more than the propagation over the rooftop, even after a far reflection.

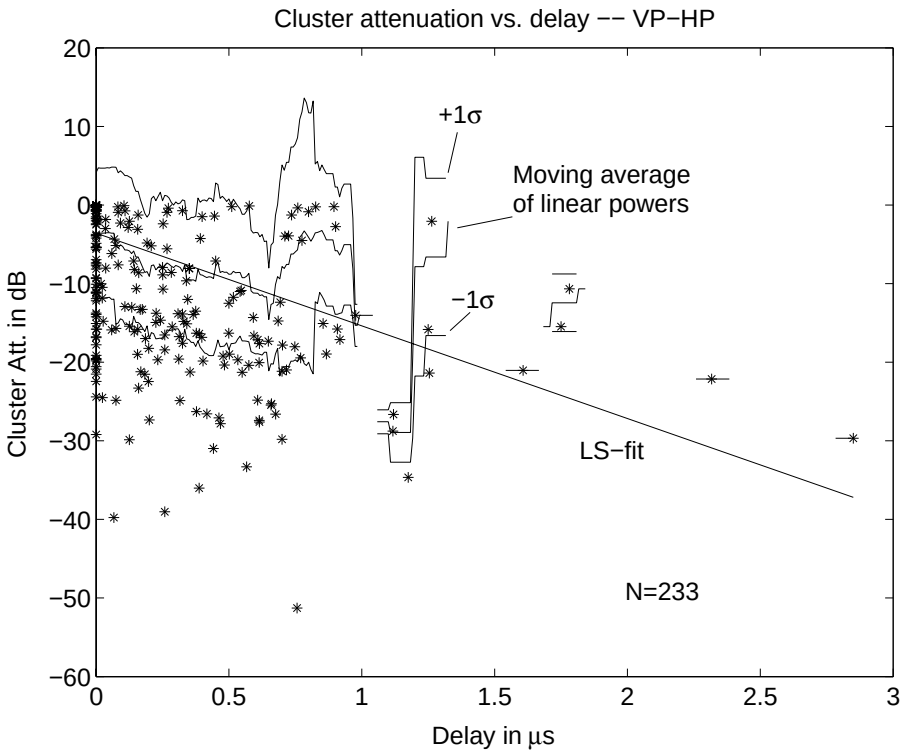

Fig. 16. Relation of the cluster power to the total power vs. delay, all TX-positions, Cross-Polarization. N is the number of clusters.

D. Relative Class Powers

To estimate the significance of different propagation mechanisms that underlie the measurements, we calculate the relative power sum that occurs in the clusters of the three different classes defined in Sec. III-C. This power was related separately for each TX-position to the associated total power. We distinguished between the three base station sites and the two polarizations, to compare the different environments. Table IV lists the relative class powers for each RX-site and polarization. At RX 1 and RX 2 (below and at the rooftop), only class 1 clusters play a significant role (street guided propagation) with 93 to 97% of the total received power. Class 2 and class 3 (over the rooftop propagation) is negligible. Especially the broad Kaisaniemenkatu street directly in front of RX 2 dominates its environment by over 97% for the more important co-polarized component.

The antenna array at site RX 3 shows a different behavior. Here, the classes 2 and 3 in general become more important. The relative contribution of class 3 is 25 to 100 times stronger at RX 3 than at RX 1 and RX 2. This is due to a large cathedral that acts as a major far reflector for the RX3 site. The relative power of horizontally (cross-) polarized waves (VP-HP) is significantly higher than for vertical (co-) polarized (VP-VP), in clusters of classes 2 and 3. Note that this behavior is true only for the relative power. The absolute power of the vertical component of the classes 2 and 3 is still $5 - 7dB$ higher than that of the horizontal components.

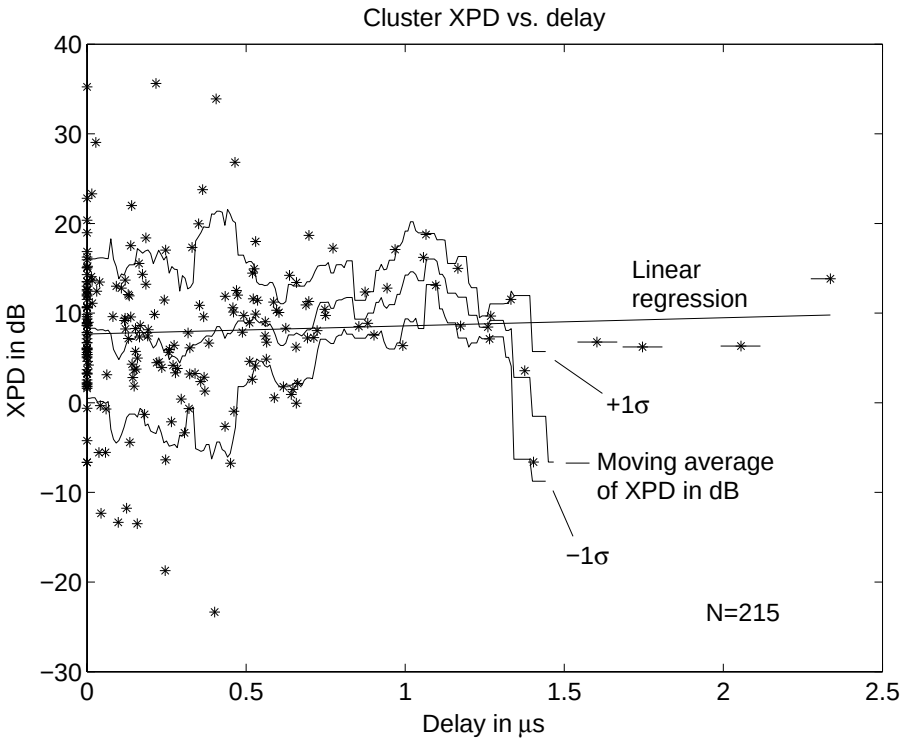

Fig. 17. Cross Polarization Discrimination (XPD) vs. delay, all TX-positions. N is the number of clusters.

E. CDF of the number of clusters

We now explore the distribution of the number of clusters, i.e., we investigate how many clusters are seen by the base station. Remember that we transmit from the MS only vertically polarized.

Figure 19 shows the cumulative distribution function of the number of clusters that are seen by the base station for all available RX- and TX-positions. The total number of clusters that we identified was 273. Separately for the three classes 1–3, we identified 119, 48, and 106 different clusters, resp. In no case there are less than 2 clusters, the most probable number of clusters is 3. On average, the base station has to handle 3.8 clusters and the upper bound is 8 clusters. Note that the maximum number of clusters depends on the classification we made by visual inspection of the results (see Section III-C) – there are always some weak waves left that are hard to assign to clusters. The difference of the power captured by the clusters to the total received power – that can be calculated e.g. by means of the spatial integral over the whole angular range – was less than $1.5dB$.

Additionally, the cdf's are shown separately for the three classes. The behavior for street guidance and far-reflection (classes 1 and 3) is similar to the global behavior. But clusters of over-the-rooftop direct propagation are rare. In 90% of the cases there is only one or even no cluster at all present in class 2.

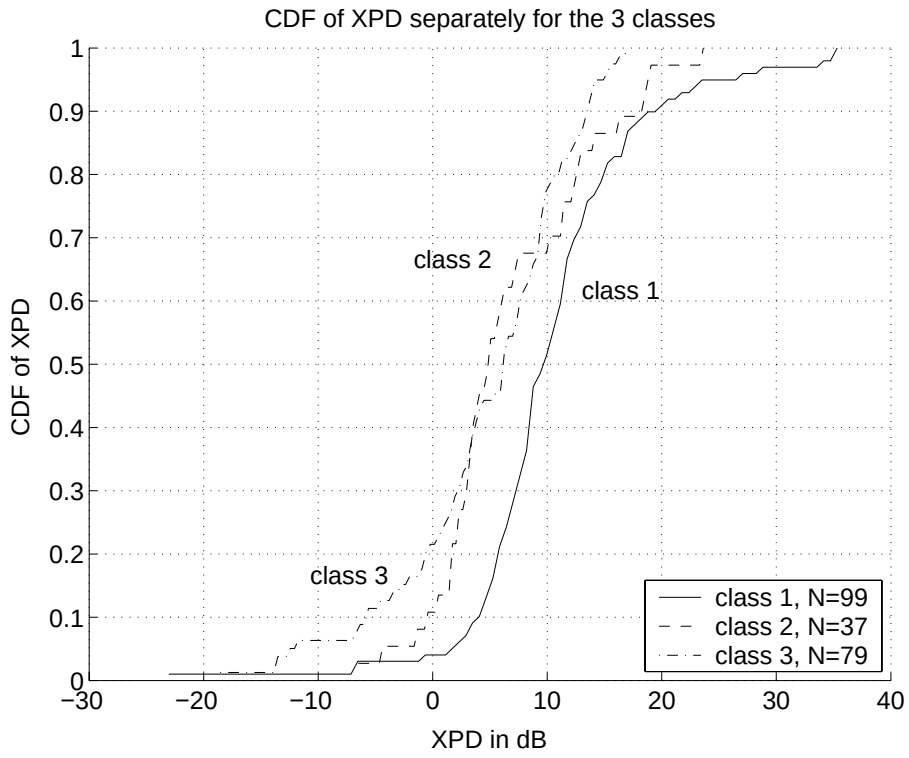

Fig. 18. CDF of the Cross Polarization Discrimination (XPD) separately for the three classes. N is the number of clusters.

V. Summary and Conclusions

We report statistical evaluations of directionally resolved impulse responses measured at 80 different TX positions and 3 different RX (BS) sites. The impinging energy is concentrated in clusters that are distinct in the azimuth-, elevation-, or delay-domains. Clusters, which are well identifiable in connection with the city map, group together several individual waves that are separable by super-resolution methods. The environment of the base station has more influence on the location of the clusters – especially in the azimuth-elevation plane – than the exact position of the mobile station.

The cluster powers decrease exponentially with increasing delay by about $8.9dB/\mu s$. Their standard deviation from this exponential law is independent of the delay, its value is $9.0dB$. While the average relative power of the strongest cluster is 83% of the total power, it is only 41% for the quasi line-of-sight components, which arrive first at the receiver.

We also investigate how many clusters are required to collect the main part of the total received power. The cumulative distribution function (cdf) of the relative power shows that in 90% of all cases we get at least 55% of the co-polarized component within the strongest cluster and 75% within the two strongest clusters. From this we can conclude that pointing only a single beam – whose beam width has to be adapted to the extent of the corresponding cluster – from the BS towards the strongest cluster, we will lose $2.6dB$ of the total available power and only $1dB$ when pointing two

RX	Class	hor. Power % of Total Power	vert. Power % of Total Power
1	1	96.5%	95.7%
	2	2.4%	3.8%
	3	1.1%	0.4%
2	1	93.5%	97.2%
	2	4.0%	2.7%
	3	2.5%	0.1%
3	1	46.7%	78.0%
	2	37.2%	12.8%
	3	16.0%	9.2%

TABLE IV

Averaged Class Powers of RX1, RX2, and RX3

beams to the two strongest clusters. Using more than two clusters hardly increases the received power.

Later clusters have in general a higher cross polarization discrimination (XPD) than shorter delayed ones, on average over all clusters the XPD is $8dB$. An interesting behavior is that reflections from higher locations (elevation $> 0°$) tend to have lower XPD.

We observe that street-guided propagation dominates the received power, as long as the base station is below or at the rooftop level. In that case the relative importance of these clusters is at least 90% of the received energy. If the BS is higher than the rooftop-level of the surrounding buildings, the relative importance of over-the-rooftop components increase from less than 5% to $10-40\%$ (depending on the polarization). Reflections from far, high buildings become stronger if these buildings have a line-of-sight (LOS) connection to the receiver. Nevertheless the street-guided propagation always dominates.

In 90% of the cases, there are at most six clusters seen by the base station, whereas the most probable number of clusters is three. The importance of class-2 clusters (direct over the rooftop) is significantly lower than for other propagation mechanisms. Both the number of such clusters and their relative power are almost negligible.

In general, we conclude that due to the limited number of clusters and the concentration of the received power in

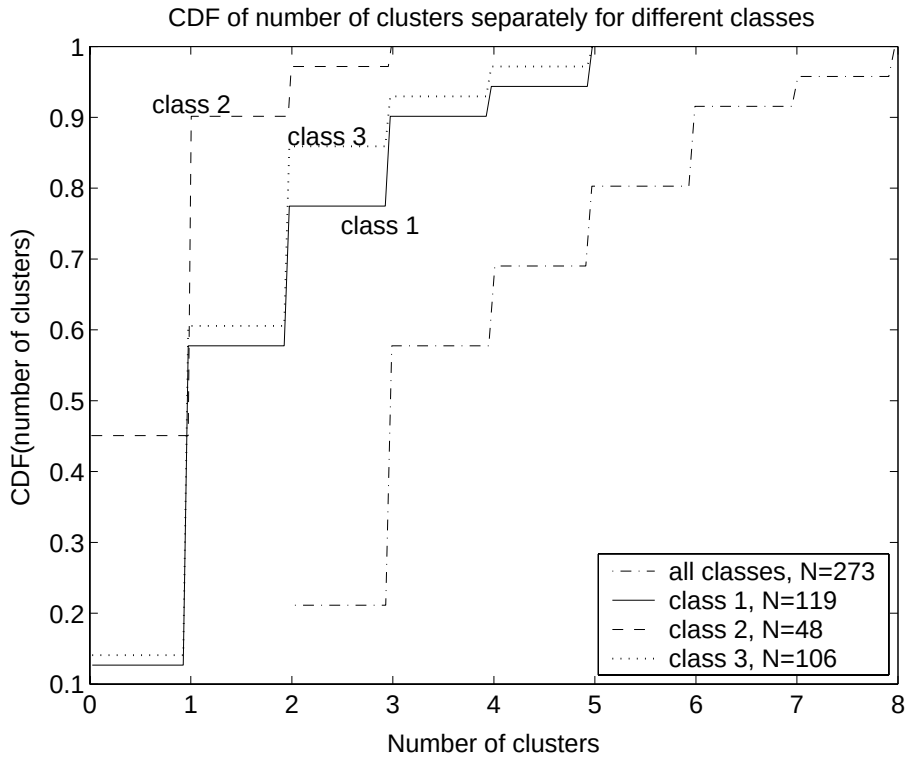

Fig. 19. CDF of the number of clusters; total number of clusters N=273. All clusters regardless of the class and separately for the three classes. N is the number of clusters in a particular class.

the two strongest clusters, an adaptive antenna base station equipped with 4–6 antennas is able to collect most of the mobile's power up to a loss of about $1dB$. Our XPD-investigations show that polarization diversity will not lead to an increased diversity order as long as the TX polarization is vertical.

Appendix

I. Least Squares Estimator of Propagation Coefficients

The vector $\vec{P}$ contains the powers of the clusters, the vector $\vec{\tau}$ denotes the corresponding mean delays. A particular cluster i's mean delay is τ_i, it's power is P_i. Note that the power is given linear, not in dB. We model the relation between the delays $\vec{\tau}$ and the powers $\vec{P}$ as exponential

$$P_n \propto P(\tau_n) = ae^{-\tau_n/b} \quad . \tag{1}$$

The parameter b denotes the the power decrease of the clusters per delay unit, and a shifts the whole exponential function up or down. I.e., a corresponds to the average attenuation of all clusters that have a delay of $0ns$. We collect

a and b into the parameter vector $\vec{\theta}$,

$$\vec{\theta} = \begin{pmatrix} b \\ a \end{pmatrix}$$

and separate the estimation problem into a non-linear problem for b and a linear problem for a. The estimated signal becomes

$$\vec{s}(\vec{\theta}) = \mathbf{H}(b) \cdot a \ , \tag{2}$$

where

$$\mathbf{H}(b) = e^{-\vec{r}/b} \ . \tag{3}$$

In our particular case $\mathbf{H}$ reduces to a $N \times 1$ matrix. The least squares estimator for $\vec{\theta}$ reads as follows:

1. b fix: $\hat{a}_{LS} = \hat{a}_{LS}(b) = \left(\mathbf{H}^T\mathbf{H}\right)^{-1}\mathbf{H}^T\vec{P}$
2. $\hat{b}_{LS} = \arg\max_b \left\{ \vec{P}^T\mathbf{H}\left(\mathbf{H}^T\mathbf{H}\right)^{-1}\mathbf{H}^T\vec{P} \right\}$

Having $\hat{b}_{LS}$, we are able to calculate $\hat{a}_{LS} = \hat{a}_{LS}(b)$. The non-linear operator $\mathbf{H}$ usually does not allow a closed-form expression of $\hat{b}_{LS}$, but as it is a one-dimensional parameter-vector, a grid search is easily implemented.

We define the logarithmic estimation error $\vec{v}$ as

$$\vec{v} = 10\log\vec{P} - 10\log\vec{s}(\vec{\theta}) \ , \tag{4}$$

and its standard deviation σ_v as

$$\sigma_v = \sqrt{\mathrm{var}\left\{\vec{v}\right\}} \ , \tag{5}$$

because then it is the standard deviation of the underlying log-normally distributed fading process.

References

[1] A. Paulraj and C. Papadias, "Space-time processing for wireless communications," *IEEE Signal Processing Magazine, no. 6*, vol. 14, pp. 49–83, Nov. 1997.

[2] S. C. Swales, M. Beach, D. Edwards, and J. P. McGeehan, "The performance enhancement of multibeam adaptive base-station antennas for cellular land mobile radio systems," *IEEE Trans. on Vehicular Technology*, vol. 39, pp. 56–67, Feb. 1990.

[3] F. Adachi, M. Sawahashi, and H. Suda, "W-CDMA: Performance evaluation and future enhancement," in *Proc. of European Personal Mobile Communications Conference (EPMCC '99), Paris*, pp. 429–434, 1999.

[4] J. C. Liberti and T. S. Rappaport, *Smart Antennas for Wireless Communications*. Prentice Hall, 1999.

[5] R. B. Ertel, P. Cardieri, K. W. Sowerby, T. S. Rappaport, and J. H. Reed, "Overview of spatial channel models for antenna array communications systems," *IEEE Personal Comm.*, vol. 5, no. 1, pp. 10–22, Feb. 1998.

[6] M. Steinbauer and A. F. Molisch, *Spatial Channel Modeling*. In Luis H. Correia (ed.), Wireless Flexible Personalized Communications – COST 259: European Co-operation in Mobile Radio Research, Wiley, to appear 2001.

[7] U. Martin, J. Fuhl, I. Gaspard, M. Haardt, A. Kuchar, C. Math, A. F. Molisch, and R. Thomä, "Model scenarios for direction-selective adaptive antennas in cellular mobile communication systems - scanning the literature," *Wireless Personal Communications Magazine, Special Issue on Space Division Multiple Access*, vol. 11, no. 1, pp. 109–129, Oct. 1999.

[8] K. Pedersen, P. Mogensen, and B. Fleury, "A stochastic model of the temporal and azimuthal dispersion seen at the base station in outdoor propagation environments," *IEEE Trans. on Vehicular Technology*, vol. 49, no. 2, pp. 437–447, Mar. 2000.

[9] J. Fuhl, J.-P. Rossi, and E. Bonek, "High resolution 3-D direction-of-arrival determination for urban mobile radio," *IEEE Trans. on Antennas and Propagation*, vol. 4, no. 45, pp. 672–682, 1997.

[10] A. Kuchar, J.-P. Rossi, and E. Bonek, "Directional macro-cell channel characterization from urban measurements," *IEEE Trans. on Antennas and Propagation*, vol. 48, no. 2, pp. 137–146, Feb. 2000.

[11] K. Kalliola, H. Laitinen, L. Vaskelainen, and P. Vainikainen, "Real-time 3D spatial-temporal dual-polarized measurement of wideband radio channel at mobile station," *IEEE Trans. on Instrumentation and Measurement*, vol. 49, no. 2, pp. 439–448, Apr. 2000.

[12] J. Laurila, K. Kalliola, M. Toeltsch, K. Hugl, P. Vainikainen, and E. Bonek, "Wideband 3-d characterization of mobile radio channels in urban environment," *IEEE Trans. on Antennas and Propagation*, to appear.

[13] K. Kalliola, J. Laurila, M. Toeltsch, K. Hugl, P. Vainikainen, and E. Bonek, "3-D directional wideband dual-polarized measurement of urban mobile radio channel with synthetic aperture technique," in *Millennium Conference on Antennas and Propagation (AP2000)*, (Davos, Switzerland), Apr. 2000.

[14] J. Kivinen, T. Korhonen, P. Aikio, R. Gruber, P. Vainikainen, and S.-G. Häggman, "Wideband radio channel measurement system at 2 GHz," *IEEE Trans. on Instrumentation and Measurement*, vol. 48, no.1, pp. 39–44, Feb. 1999.

[15] K. Kalliola and P. Vainikainen, "Characterization system for radio channel of adaptive array antennas," in *Proc. of Int. Symp. on Personal Indoor Mobile Radio Conference (PIMRC '97), Helsinki, Finland*, pp. 95–99, 1997.

[16] R. Roy, A. Paulraj, and T. Kailath, "ESPRIT - a subspace rotation approach to estimation of parameters of cisoids in noise," *IEEE Trans. on Acoustics, Speech and Signal Processing*, vol. 32, pp. 1340–1342, May 1986.

[17] M. Zoltowski, M. Haardt, and C. Mathews, "Closed-form 2-D angle estimation with rectangular arrays in element space or beamspace via unitary ESPRIT," *IEEE Trans. on Signal Processing*, vol. 44, no. 2, pp. 316–328, Dec. 1994.

[18] M. Haardt and J. Nossek, "Unitary ESPRIT: How to obtain an increased estimation accuracy with a reduced computational burden," *IEEE Trans. on Signal Processing*, vol. 43, pp. 1232–1242, May 1995.

[19] H. Krim and M. Viberg, "Two decades of array signal processing research," *IEEE Signal Processing Magazine (Sp.Issue on Array Processing)*, vol. 13, July 1996.

[20] M. Steinbauer, D. Hampicke, G. Sommerkorn, A. Schneider, A. F. Molisch, R. Thomä, and E. Bonek, "Array-measurement of the double-directional mobile radio channel," in *IEEE Vehicular Technology Conference (VTC 2000-Spring), Tokyo*, May 2000.

[21] L. H. Correia, ed., *Wireless Flexible Personalized Communications – COST 259: European Co-operation in Mobile Radio Research.* Wiley, Mar. 2001. 512 p.

[22] Commission of the European Communities, *Digital land mobile radio communications - COST 207.* ECSC-EEC-EAEC, 1989.